Available online at: https://ijact.in

Date of Submission	03/08/2019
Date of Acceptance	02/09/2019
Date of Publication	03/10/2019
Page numbers	3374-3387(14 Pages)

Cite This Paper: Mike G, Larry Pearlstein, Tyler Daws, Ezekiel S, Alshehri AA. A Comparative Study of Multi-Focus, Multi-Resolution Image Fusion Transforms and Methods, 8(9), COMPUSOFT, An International Journal of Advanced Computer Technology. PP. 3374-3387.

ISSN:2320-0790

COMPUSOFT
An International Journal of Advanced Computer Technology

A COMPARATIVE STUDY OF MULTI-FOCUS, MULTI-RESOLUTION IMAGE FUSION TRANSFORMS AND METHODS

Mike Giansiracusa[1], Larry Pearlstein[2], Tyler Daws[1], Soundararajan Ezekiel[1] and Abdullah Ali Alshehri[3],

[1]Indiana University of Pennsylvania Indiana, Pennsylvania
[2]The College of New Jersey Ewing, New Jersey
[3]King Abdulaziz University, Jeddah, Kingdom of Saudi Arabia

Abstract: Multi-resolution image decomposition transforms are a popular approach to current image processing problems such as image fusion, noise reduction, and deblurring. Over the past few decades, new algorithms have been developed based on the wavelet transform to remedy its directional and shift invariant shortcomings (undecimated discrete wavelet transform is shift invariant). This study provides a comprehensive analysis of multi-focus image fusion techniques using six different multi-resolution decomposition transforms to determine the optimal transform for an image fusion application. The transforms investigated are the wavelet, double-density wavelet, dual-tree wavelet, curvelet, contourlet, and bandelet. Furthermore, for each transform, seven transform coefficient fusion algorithms are analyzed and the performance is evaluated using eight no-reference objective image fusion metrics. The transforms and algorithms selected are applied to a data set that has 27 pairs of multi-focus source images used for image fusion. By bringing together the transforms, fusion algorithms, and metrics presented in this study as derived separately from different authors, the study seeks to compare these methods. However, a complete comparison amongst the different transforms, algorithms, and metrics has not been found in any of the existing literature. Our goal is to provide useful insight into their applications in image fusion. The summary of the aggregated results indicates that (1) the curvelet is the most robust transform, (2) down-up and linear are the most effect methods of fusion, and (3) Tsallis is the best metric for multi-focus image fusion.

Keywords: Bandelet; Contourlet; Curvelet; Double Density Wavelet; Dual-Tree Wavelet; Multi-Focus Image Fusion; Multi-Resolution; No Reference Objective Image Fusion Metrics; Wavelet.

I. INTRODUCTION

Multi-resolution image decomposition transforms have recently been studied for use in a significant number of applications. Wavelet transform, for example has been used in the JPEG2000 standard for image compression. Adaptations of the wavelet for image compression are still being explored, but currently the wavelet incurs less information loss during compression than previous algorithms such as JPEG-LS or JPEG 2000 (arithmeticcoding and zero tree related to independent random variables, stuff all the entropy into the independent random variable) [1, 2, 3, 4]. Wavelets have also been used in edge detection, andcompared to its predecessor, the Fourier transform, the wavelet has characteristics for edge detection within images and scaling capabilities [5]. Implementation of the wavelet transform for different applications is based on the wavelet coefficients.Wavelet analysis has been used in noise reduction for images and signals [6]. However, the basic fully decimated discrete wavelet transform (DWT) has certain weaknesses – it is not shift-invariant and is less effective at representing image features aligned at oblique angles. Therefore, extensive research has been conducted to further improve upon the wavelet [7, 8].

Several new algorithms have been developed recently that each improve upon the basic DWT in certain applications. For example, the double-density wavelet has the advantage of

being nearly shift-invariant [9]. The Dual Tree Complex Wavelet Transform is also nearly shift invariant, and has improved directional sensitivity to edges compared with the conventional DWT. The curvelet was designed similarly to these two, based on the ridgelet, in the continuous domain, to better exploit smooth contours within an image for denoising applications [10, 11]. Contourlets also exploit smooth contours; however, they do so in the discrete domain [12]. The discretization of the contourlet directionality coefficients makes them useful in image denoising applications [13]. Bandelets exploit the geometric flow of the image to provide an orthogonal basis for wavelet functions that is along the direction of the geometry in localized regions [14, 15, 16].

The aforementioned transforms have been investigated as alternatives to the DWT for various applications, in attempts to improve performance and capture image information more efficiently. The applications for which these alternatives are particularly effective are deblurring, metric construction, object segmentation, and image fusion. Both the contourlet and curvelet have been applied to signal denoising [17], and the contourlet was also used to create a no reference blur metric [18]. The contourlet has been used to complete multi-modal image fusion [19]. The Double Density wavelet has been used for speckle reduction [20], and object detection [21]. The Dual Tree wavelet has been used for image enhancement [22], facial recognition [23], and video coding [24]. The Double Density wavelet and the Dual Tree wavelet have been exploited together to construct no-reference blur metrics [25]. Some of the more recent studies used the Bandelet. The Bandelet has been used in combination with a one-dimensional wavelet transform for image denoising [5, 26], for compression and approximation [15], and image fusion [16, 43]. There is a surfeit of reports on the characteristics of these algorithms, but there is need for a framework for choosing among them for a given application. Some applications are intended to produce a result that is useful and/or aesthetically pleasing for a human viewer. Ideally such applications would be studied through the use of extensive subjective viewing trials. Unfortunately, subjective evaluation is often infeasible – either because the data sets are too massive, or because subjective evaluation is inherently complex and unrepeatable. Accordingly, it is highly desirable to have objective metrics that closely track rigorous subjective evaluations. To date there has been no comprehensive evaluation of objective image metrics over the different algorithms for image fusion considered here. The goal of image fusion is often to provide a result that is maximally useful for a human analyst and it is desirable to have objective metrics that track well with this subjective activity.

Another challenge within the field of image fusion arises from the fact that different results have been reported for a given fusion technique based on the type of data considered [27]. For example, a fusion-denoising algorithm might work well for multi-modal images and yet work poorly for multi-focus images. Figures 1 and 2 show examples of both multi-model image fusion and multi-focus image fusion. A better understanding of the relative merits of different algorithms for image fusion would be of great value. Additionally, there would be value in the validation of objective metrics for the specific application of image fusion. This is complicated by the many different types of inputs, transform coefficients and fusion methods that must be considered.

Visible Infrared Fused

Figure 1: Multi-Modal Image Fusion

Foreground Background Fused

Figure 2: Multi-Focus Image Fusion

A common metric for evaluation of an image fusion algorithm is based on the receiver operating characteristic (ROC) analysis [28, 40]. In this study, we focus solely on multi-focus imagery data and use six different transforms to perform image fusion. We assess these transforms with ten objective metrics that were described by Liu et al. [29]. These metrics can be classified into four categories: information theory-based, image feature-based, structural similarity-based and human perception based. The purpose of this study is to identify the most suitable methods for multi-focus image fusion by evaluating the performance of several popular methods via an array of metrics. It is our hope that this study serves as an archetype for future studies in image fusion.

This paper is organized as follows: Section 2 discusses the mathematical background behind the techniques used to process the data obtained for multi-focus, multi-resolution image fusion. Section 3 explains the fusion algorithms. Section 4 describes the different metrics used. Section 5 contains our experimental results, which consist of an explanation of our ranking system and the results. Section 6 details conclusions of the requirements and future directions of the algorithm comparisons.

II. MATERIALS AND METHODS

2.1 Multi-Resolution Transform

Amongst the six transforms described below there is a general commonality among them. Figure 3 shows a generic block diagram that applies to many fusion algorithms, where a transform decomposes an image into coefficients.

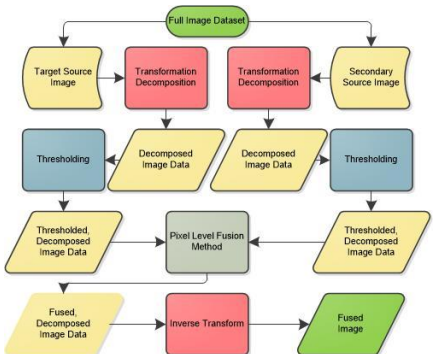

Figure 3. Transform-Based Image Fusion Block Diagram

How this decomposition occurs differs among each transform. Depending on the transform, the study will produce the same number of coefficients as there are pixels, or more/fewer coefficients than pixels. For the purpose of denoising or de-blurring, thresholding often occurs in the coefficient domain, and the image is reconstructed from the thresholded coefficients. All the types of image fusion presented in this paper occur in the coefficient domain. In fact, there are often different categories of coefficients, for example approximatecoefficients and detail coefficients, which can be fused in different manners. For example, the detail coefficients of an image could be fused by taking the means of pairs of coefficients from two images. In that same image, the approximate coefficients could be fused by taking the maximum coefficient value from pairs of coefficients. After fusion occurs at the coefficient level, the inverse transform is used to produce the fused image. The rest of this section provides the motivation for each transform along with its detailed description.

2.1.1 Wavelet

A wavelet is defined as a finite wave like oscillation that has an average value of zero.Moreover, a wavelet begins with an amplitude of zero and will increase and decrease in amplitude a finite number of times before ending with a final amplitude of zero.For a function, $\psi(x)$, to be considered a wavelet, the following two conditions must hold:

$$\int_{-\infty}^{\infty} \psi(x)\,dx = 0 \tag{1}$$

$$\int_{-\infty}^{\infty} \frac{|\hat{\psi}(\omega)|^2}{\omega}\,d\omega = C_{\psi} < \infty \tag{2}$$

Where, $\Psi(\omega)$ is the Fourier transform of the selected wavelet function and C_{ψ} is the *admissible constant*. There have been numerous wavelets constructed, most derived from Daubechies[7], which can be categorized according to whether the wavelets are defined on a discrete grid vs. over continuous time or space, and whether they are real vs. complex valued.Two fundamental characteristics of wavelets are their rescale and translation definitions.Given a mother wavelet $\Psi(x)$, an entire family of wavelets $\psi_{j,k}(x)$ is defined as:

$$\psi_{j,k}(x) = \frac{1}{\sqrt{|j|}}\psi\left(\frac{x-k}{j}\right) \tag{3}$$

where j is the scaling variable and k is the translation variable. The rescale and translational characteristics of the wavelet allow it to detect small abrupt changes in signals, which makes it an ideal transform for point-wise edge detection.

The continuous wavelet transform(CWT), defined as the inner product of a function $f(x) \in L2(\mathbb{R})$and a Wavelet $\Psi(x)$, is expressed

$$f, \psi_{j,k} = \int_{-\infty}^{\infty} f(x)\frac{1}{\sqrt{|j|}}\psi\left(\frac{x-k}{j}\right)dx \tag{4}$$

In the field of image processing, the function f would represent an image that has the wavelet transform applied to it.However, images are not generally processed as continuous-space functions, but rather as sampled (discrete space) functions.As a result, the discrete wavelet transform (DWT), not the CWT, is generally used to process sampled images.Similar to the CWT, thediscrete wavelet transform of the function f, which we will denote G_{ψ}, can be expressed as

$$G_{\psi}(f,\psi) = \frac{1}{\sqrt{M}}\sum_{n} f(n)\psi_{j,k}(n) \tag{5}$$

Where, M is a scaling weight. We note that there are some drawbacks as a result of moving from a continuous to discrete transformation.In the discrete domain, the wavelet transform loses directionality and shift-invariance.Hence, the wavelet can detect image edges, but does not see an entire contoured edge as one connected piece. Lack of shift-invariance refers to the discrete wavelet transform's inability to transform shifted versions of the function f in the time domain as shifted versions of G_{ψ} in the wavelet domain. These two shortcomings sparked the creation of multiple other multi-resolution transforms which attempt to outperform the DWT.

2.1.2 Contourlet Multi-Resolution Transform

The contourlet transformation was originally proposed by Minh N. Do and Martin Vetterli in 2002 in response to the directional and anisotropic constraints of the wavelet and curvelet [12]. The contourlet includes basis elements that cover more directions than the standard wavelet of just horizontal, vertical, and diagonal. The basic two-dimensional wavelet transform provided interesting multi-resolution and localization features, but lacked the ability to efficiently model local edge direction and curvature [32]. The contourlet is composed of two processing stages: a Laplacian pyramid and a directional filter bank. The contourlet is able to effectively represent images by combining five desirable properties: anisotropy, directionality, multi-resolution, locality, and the ability to process sampled data. A major advantage of the contourlet transform compared to the curvelet transform is that the contourlet transform was specifically developed for the discrete domain. Unlike the wavelet, which grew from a one-dimensional signal transformation, the contourlet was designed specifically for image processing [12].

2.1.2.1 Laplacian Pyramid

To simplify the description of the Laplacian pyramid let us assume an input image pixel resolution of 2^j x 2^j pixels. The Laplacian pyramid can be considered as a series of error images that are the result of differences in a Gaussian pyramid structure. A Gaussian pyramid is constructed by passing an image,*I*,through a low-pass filter and then down-sampling the image by a factor of 2 in each dimension, so that it now has resolution 2^{j-1} x 2^{j-1} pixels. This filtering and down sampling is done for consecutive levels to create a pyramid[12]. Hence, for example, if an original image was 512 x 512, then the second level of the Gaussian pyramid would be size 256 x 256, the third level would be 128 x 128, etc. The Laplacian pyramid is then constructed as follows

$$L_i = G_i - U\{G_{i+1}\} \qquad (6)$$

where L_i is the i^{th} level of the Laplacian pyramid, G_i is the i^{th} level of the Gaussian pyramid, and $U\{G_{i+1}\}$ is the up sampled $i+1$ level of the Gaussian pyramid. As the method progresses down the Laplacian pyramid, the amount of edge information lost increases (with a corresponding error increase). Finally, if there are *n* levels in a given Gaussian pyramid structure, then we define L_n as follows

$$L_n = G_n \qquad (7)$$

The Laplacian pyramid is an essential part of the contourlet transform because the difference images that it produces highlight local characteristics within the source image [12]. The identification of important features within an image, such as edges, is used in combination with thresholding operations, which can be applied to the contourlet coefficients. Figure 4 shows an example of a Laplacian pyramid of the Lenna image with four levels.

Figure 4. Laplacian pyramid of Lenna

2.1.2.2 Directional Filter Bank

The Directional Filter Bank (DFB) provides the contourlet transform with the anisotropic and directional capabilities that the wavelet transform lacks, as shown in Figure 5. A wavelet filter bank is the basis for the contourlet's DFB. Let *n* represent the number of levels within the DFB; when $n=0$ the DFB is simply a wavelet filter bank.

At higher levels of *n*, a two-channel quincunx filter bank with fan filters is used to divide an image into two directions, vertical and horizontal [12]. A shearing operator then allows for different directions, such as $30°$ or $60°$ to become the vertical edge for which the image is then dived into an additional two directions. Hence the DFB actually allows for directional decomposition of an image into 2^ndifferent directions where *n* is an integer greater than two.

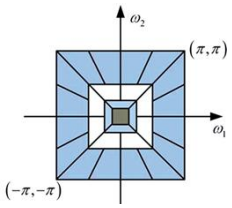

Figure 5. Contourlet DFB

Note that a general wavelet filter bank only allows for image decomposition in three directions; horizontal, vertical, and diagonal because it is defined as $\pi/2^k$ where k is an integer. The sampling matrices used within the DFB have the following form:

$$S_k^{(l)} = \begin{cases} diag\left(2^{l-1}, 2\right), for\ 0 \le k < 2^{l-1} \\ diag\left(2, 2^{l-1}\right), for\ 2^{l-1} \le k < 2^l \end{cases} \qquad (8)$$

where *j* is the level of directional decomposition of the DFB and *k* is the given sampling matrix index [12]. Together the directional filter bank and the Laplacian pyramid are often referred to as a Pyramidal Directional Filter Bank (PDFB). The contourlet transform itself is then a combination of capturing high frequency information from the DFB and low frequency information from the Laplacian pyramid to extract the most salient information from the contourlet coefficients. The discrete contourlet transform first applies the Laplacian pyramid on a given image *I*, and then each level of the Laplacian pyramid is passed through the DFB. The result is an image decomposed into multiple directional sub-bands at numerous scales. Figure 6 shows the discrete contourlet filter bank that Vetterli and Do used in their discussion [12].

The contourlet has seen numerous applications since its inception in 2005. Many of these applications deal with denoising of images [33, 34]. The contourlet, as expressed above, is an attractive choice of transform for denoising situations where there are many well defined contours within an image. Furthermore, the contourlet has been used in de-blurring applications and construction of blur metrics [35, 36]. Finally, like the wavelet, the contourlet has been used in applications for image fusion, where fusion occurs at the coefficient level [37].

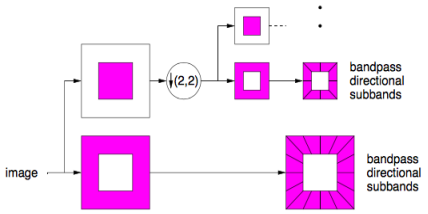

Figure 6. Vetterli and Do's Contourlet Filter Bank

2.1.3 Double Density Wavelet

The Double Density Wavelet (DDW) [20, 9] is one of the many transforms that attempt to fix one of the DWT's major problems: lack of shift-invariance. It is ideal to have a multi-resolution transform that is shift-invariant so that the coefficients produced can be directly used to identify image features and their locations. The double density wavelet structure gives "near" shift-invariance which is a large improvement over the critically sampled DWT. In fact, the double density wavelet approximates the continuous wavelet quite well as compared to the separable DWT.Based on applying two distinct wavelets and a single scaling function,the double densitywavelet has a greater density of coefficients than the fully-decimated DWT.The two wavelets selected in the DWT are chosen so that they are to be offset from one another by a factor of one-half.Furthermore, both the scaling function $\phi(t)$ and the two wavelet functions $\psi_1(t)$ and $\psi_2(t)$ will satisfy the following dilation and wavelet equations

$$\phi(t)=\sqrt{2}\sum_n h_0(n)\phi(2t-n) \qquad (9)$$

$$\psi_i(t)=\sqrt{2}\sum_n h_i(n)\phi(2t-n) \quad i=1,2 \qquad (10)$$

Where, $h_0(n)$ is a scaling (low-pass) filter and the $h_i(n)$ are wavelet (high-pass) filters. The filters used within the decomposition are finite impulse response (FIR) filters that provide perfect reconstruction of a signal in one dimension.These filters are selected to be an oversampled filter bank, and maintain the same amount of redundancy within eachsampling level.The name "double-density" is derived from the filter's oversampling rate.If the filter bank is iterated once, the oversampling rate is $\frac{7}{4}$. As iterations continue, the oversampling rate approaches two, hence the term double density.No matter how many levels of iteration are used, the oversampling rate of the one-dimensional DDW will not exceed two.The double-density wavelet has a higher redundancy than a Laplacian pyramid, described above in the contourlet Section,but a lower redundancy than the dual tree wavelet, described below.

The DDW redundancy however is an explanation for the one-dimensional double density wavelet. The comparison of the different transform redundancies still holds for two-dimensions, but the double density wavelet is now redundant by a factor that approaches $\frac{8}{3}$.The two-dimensionaldouble densitywavelet is constructed by alternating between rows and columns using one-dimensional double densitywavelets.Thetransform itself is similar to the separable DWT in two dimensions, with its dyadic structure.While the double density wavelet represents an improvement over the DWT it has the drawbacks of relatively high coefficient redundancy and relatively poor representation of arbitrarily oriented edges. Because the analysis only makes use of vertical and horizontally oriented filters the transform's ability to model oblique edge orientation is similar to that of the basic DWT. Hence, even though the DDW partially addresses the issue of shift-invariance, it still lacks the ability to efficiently model arbitrary edge orientations.

2.1.4 Dual Tree Wavelet

The Dual Tree wavelet (DTW) gets its name from its dual filtering system it uses to produce coefficients, where the tree describes the structure of wavelet coefficient branching [2]. The ultimate goal of a dual tree wavelet transform is to use wavelets that are analytic. However, the wavelets are required to have compact support and as a result, can never achieve a truly analytic wavelet for image processing applications. Hence the dual tree wavelet transform uses an approximation of an analytic wavelet [38]. For the DTW transform a signal or image is broken down using two separate two-channel filters. Each filter has its own low-pass (scaling) and high-pass (wavelet) filter. Figure 7 displays the filter bank system implemented in the dual tree wavelet scheme.

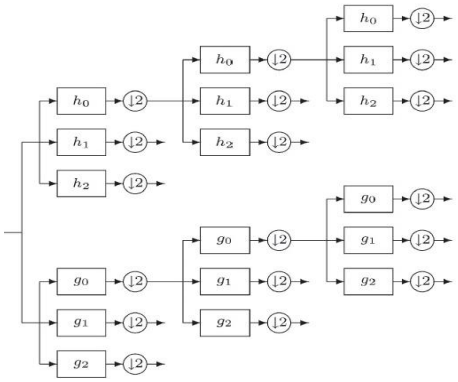

Figure7. Dual Tree Filter bank - $h_0(n)$ and $g_0(n)$ are low-pass while $h_1(n)$ and $g_1(n)$ are high-pass and $h_2(n)$ and $g_2(n)$ are the approximate

The essential part to the filters selected is that the filter bank of one tree must generate a wavelet and scaling function that is a Hilbert transform pair of the functions generated from the other tree.Here the Hilbert Transform of a function $f \in L^2(\mathrm{R})$ is defined as

$$\mathrm{F}\left\{\mathrm{H}\left(f(x)\right)\right\}=-i\,\mathrm{sign}(x)\,\hat{f}(x) \qquad (11)$$

where $\hat{f}(x)$ is the Fourier transform of the function *f*.Furthermore, a Hilbert pair is then defined as

$$f' = \mathrm{H}f \tag{12}$$

Where, we denote the Hilbert transformed function as f'. In choosing filters that result in wavelets that form Hilbert pairs, it ensures that the wavelets will be orthogonal to each other and hence makes finding an orthogonal wavelet basis easier. Furthermore, since images can be thought of as matrices with only real values, then the implementation does not use the complex portion of any wavelet.

Once the image is fed through the DTW filter banks, the resulting scaling and wavelet functions are used to decompose the image into coefficients.A drawback of the DTWtransform is that it is rather redundant compared to other transforms.For each dimension, there a dual treesystem.Hence, for a one-dimensional signal there are two sets of filter banks, but for a two-dimensional image there are four sets of filter banks.This type of structure causes the dual tree wavelet to have 2^d redundancy of the coefficients where d is number of dimensions.It is important to note that the dual tree wavelet and the double density wavelet are often used in conjunction. This is sometimes referred to as the double density dual tree discrete wavelet transform or D3TDWT for short. In this study, the DDW and DWT were analyzed separately to better understand the advantages and disadvantages of each.

2.1.4 Curvelet

The curvelet was constructed to be an extension of the wavelet transform similar to the other methods such as the double density wavelet and the dual tree wavelet. The difference between the curvelet and the aforementioned transforms is that the curvelet takes advantage of the ridgelet transform [30] instead of a wavelet transform. Furthermore, the curvelet was specifically designed to detect smooth curving edges within an image. Ridgelets exploit wavelet like functions to better represent smooth edges within a global context, but does not provide significant local information. Ridgelet functions not only have scale and translation characteristics to them, but they also have an orientation characteristic which assists in exploiting smooth edge data.

A limitation of the ridgelet transform is that it is applied in a global context, hence the idea naturally came about to partition a given domain and then apply the ridgelet transform on each of those sub sections.This idea gave rise to the curvelet transformation. The continuous curvelet transformation works in the frequency domain, and uses polar coordinates to help tile the domain into sub sections. Each section is split into wedges by taking a series of concentric circles such that the number of wedges, *N*, associated with one of the concentric circles is:

$$N_j = 4 \times 2^{\frac{j}{2}} \tag{13}$$

where *j* corresponds to the number of concentric circles. See the Figure 8below for an example of how the frequency domain is tiled.

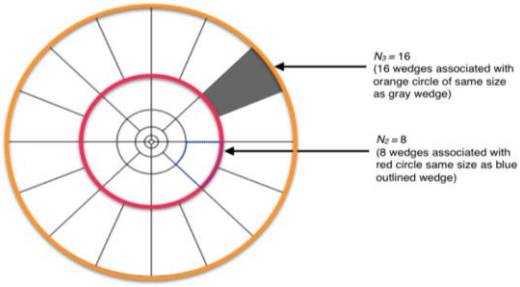

Figure 8. Continuous Curvelet Tiling

A curvelet itself is obtain through bandpass filtering of multi-scale ridgelets, which is formally defined as:

$$\psi_{a,b,\theta}(x) = a^{\frac{-3}{4}} \psi\left(M_a R_\theta (x-b)\right) \tag{14}$$

where ψ is a wavelet function, a is a scaling variablebetween zero and one, b is a translation variable, and Θ represents an orientation. Furthermore,R_Θ represents a rotation and M_a is the following scaling matrix:

$$M_a = \begin{bmatrix} 1/a & 0 \\ 0 & 1/\sqrt{a} \end{bmatrix} \tag{15}$$

The aspect ratio of each wedge is approximately the width equal to the length squared.The curvelet transform itself is a map from $L^2(\mathrm{R}^2) \to F$ where F is the frequency domain and L is the Laplacian operator. The transform itself has a similar structure to the wavelet transform and is expressed as

$$\psi_{a,b,\theta}, f = \int_{\mathrm{R}^2} \psi_{a,b,\theta}(x)\, f(x)\, dx \tag{16}$$

where f is the function to decompose the data (generally an image) into components. Unfortunately, the transform is defined in the continuous domain, whereas a discrete version is required for image processing. For the curvelet transform being applied to a sampled image, *f*, the frequency domain cannot be tiled using concentric circles, and concentric squares are used instead. Using concentric squares makes the sizes of corresponding wedges slightly different and thus the orientations and rotations no longer reflect the physical scene or natural representations. Hence, in place of rotation, shearing operators are used to remedy the discrete curvelet transform's performance capabilities. The discrete curvelet transform as [17, 10, 11]

$$F_\psi(f,\psi) = \sum_n f(n) \psi_{a,b,\theta}(n) \tag{17}$$

The curvelet transform represented an advance as a directional multi-resolution transform; however, it was not widely used the field of image processing, as it is more naturally suited to continuous-space signals, rather than sampled signals. To remedy this shortcoming the contourlet transform was developed.

2.1.5 Bandelet

Bandelets are the most complex multi-resolution transform [14, 16, 42] among the six selected for this study. How bandelets handle the directional and anisotropic features of an image is less computationally efficient than the contourlet, but

the results, in applications such as de-noising, seem to indicate that bandelet reconstruction of images can produce higher quality images. A bandelet captures directional information, including smooth contours, using what is called geometric flow. Geometric flow refers to a vector field of parallel vectors where the local direction of a function *f* has regular variations. Bandelets exploit a very similar dyadic structure as the other transforms listed before, but the major difference is that the geometric flow defines the geometry in each section of an image rather than localization.

Once the geometry of a given image has been computed, a bandelet can be constructed by taking a local orthogonal transform of wavelet coefficients. A different transform will occur for each geometric direction found within the geometric flow. This then allows a process to find an optimal set of filters for finding the best bandelet basis. The ideal bandelet basis is an orthonormal basis created by warping anisotropic wavelet bases with respect to the geometric flow.

Bandelet decomposition is performedin such a way that the scale of resulting sub-bands is 2^j , calling attention to a singularity in a sub-section of the image, referred to as *S*. Furthermore, the wavelet coefficients $f, \psi_{j,k}$ are samples of a given regularized function which is underlying the bandelet composition by:

$$\begin{aligned} &\left\langle f, \psi_{jn} \right\rangle = f_j(2^j n) \\ &\text{where } f_j(x) \overset{\text{def.}}{=} f * \psi_j(x) \\ &\text{and } \psi_j(x) = \frac{1}{2^j}\psi(-2^{-j}x) \end{aligned} \tag{18}$$

2.1.6 General Linear Hypothesis Test

The general linear hypothesis test (GLHT) is used to determine the effectiveness of each variable in the final outcome. A general linear hypothesis refers to null hypotheses of the form H_0: K theta = m for some parametric model with parameter estimates coef(model). The generic method glht dispatches on its second argument (linfct). The matrix of coefficients K are specified directly via the linfct argument.

2.2 Fusion methods

Pixel-level image fusion is a process whereby a single composite image is produced based on two reference images [39, 41]. Many methods for multi-resolution image fusion have been advanced, which are generally distinguished by different methods for merging approximation and detail coefficients. For example, in "max-min" fusion, the max criterion is used for the approximate coefficients and the min criterion for the detail coefficients. This notation will be the convention used for all of the fusions methods except for those of the bandelet. Since the bandelet only has detail coefficients, only one fusion criterion can be used in that framework. In the following sections we will let ***F*** be the fused image, ***A*** be the first input image and ***B*** be the second input image. Additionally, the coefficients f_{ij} will form matrices, e.g., ***F***(*i*, *j*).

2.2.1 Max

The max criterion will take the maximum absolute value of each entry between the two matrices as follows:

$$f_{ij} = \begin{cases} a_{ij} & if \left|a_{ij}\right| \geq \left|b_{ij}\right| \\ b_{ij} & \text{otherwise} \end{cases} \tag{19}$$

It is important that we use absolute values in these decision statements because while pixel values cannot be negative, multi-resolution coefficients can.

2.2.2 Min

The min criterion will take the minimum absolute value of each entry between the two matrices as follows:

$$f_{ij} = \begin{cases} a_{ij} & if \left|a_{ij}\right| \leq \left|b_{ij}\right| \\ b_{ij} & \text{otherwise} \end{cases} \tag{20}$$

2.2.3 Linear

The linear method involves a linear combination of the two matrices with their coefficients summing to 1. If a constant parameter *c* is selected on the interval (0,1) then the resulting coefficient matrix will have values:

$$f_{ij} = c_{ij}a_{ij} + \left(1 - c_{ij}\right)b_{ij} \tag{21}$$

2.2.4 Mean

The mean method is a special case of the linear method where *c* = 0.5. It will take the mean between the two entries at each position in the matrix like this:

$$f_{ij} = \frac{a_{ij} + b_{ij}}{2} \tag{22}$$

2.2.5 Principal Component Analysis

Principal Component Analysis (PCA) is method that can be used to reduce the dimensions of matrices while keeping most of the information. The correlated values in the larger matrix are reduced into uncorrelated variables known as principal components. For image fusion, PCA can be used to pick out the most important features of an image and then fuse them.

2.3 Metrics

Liu, et al. [29] considered 12 different types of image quality evaluation metrics in the context of fusion of data for night vision. They organized the metrics according to four categories, which are: mutual information based, feature based, structured similarity index based, and subjective human evaluation. Since the present study seeks to evaluate objective fusion methods, the human perception based methods are omitted; and thus, the eight remaining metrics were investigated here.

2.3.1 Mutual Information

Mutual information measures the dependency between two discrete random variables. Entropy is used to define mutual information in units of bits. The mutual information between discrete random variables *U*, *V* is defined as:

$$MI(U,V)=\sum_{v\in V}\sum_{u\in U}p(u,v)\log_2\frac{p(u,v)}{p(u)p(v)} \qquad (23)$$

where $p(u, v)$ is the joint probability function and $p(u)$ and $p(v)$ are the marginal probability functions of **U** and **V** respectively.

2.3.2 Tsallis Entropy

Tsallis entropy is a divergence measure based on the degree of dependence between two discrete random variables. Tsallis entropy is a generalization of Shannon entropy, and is parametrized by a single real constant.

2.3.3 Nonlinear Correlation

Nonlinear correlation information entropy uses a nonlinear correlation matrix along with the two input images and fused image to and produces a quality metric based on the eigenvalues of this matrix.

2.3.4 Gradient-Based Fusion Performance

Gradient-based fusion performance uses the edge information from each image to evaluate the quality of fusion. The Sobel edge operator is applied to find the edge strength of the input image. Then relative strength between the input and the fused image is calculated. The edge strength and orientation preserve values that are derived and quantified. Using a weighted average of the edge information and preservation values are obtained as the metric as follows:

$$Q_G=\frac{\sum_{i=1}^{M}\sum_{j=1}^{N}[X+Y]}{\sum_{i=1}^{M}\sum_{j=1}^{N}[I+J]} \qquad (24)$$

where

$$X=Q^{AF}(i,j)w^{A}(i,j)$$
$$Y=Q^{BF}(i,j)w^{B}(i,j)$$
$$I=w^{A}(i,j)$$
$$J=w^{B}(i,j)$$

where the Q^{AF} and Q^{BF} terms are the edge information preservation values and the w terms are the weighting coefficients.

2.3.5 Multi-Scale

A two-level Haar wavelet is used to calculate the image fusion metric based on a multiscale scheme. The edge information is retrieved from the high-pass and band-pass components of the decomposition. Then a normalized performance metric at a scale s is calculated using the components to yield $Q^{\frac{AB}{F}}$. Then the final multi-scale metric is calculated by combining the measurement at different scales:

$$Q_M=\prod_{s=1}^{N}\left(Q_s^{AB/F}\right)^{\alpha_s} \qquad (25)$$

where α represents the weighted scaling factor.

2.3.6 Spatial Frequency

The spatial frequency fusion metric Q_{SF} measures the activity level of an image based on four first-order gradients along four directions. The reference gradients take the maximum of the absolute gradient values between the input images. The metric calculates the ratio of spatial frequency error as

$$Q_{SF}=\frac{(SF_F-SF_R)}{SF_R} \qquad (26)$$

where $SF=\sqrt{(RF)^2+(CF)^2+(MDF)^2+(SDF)^2}$ (27)

and F represents the fused image while R represents the calculated reference gradients' frequency.
MDF is

$$MDF=\sqrt{w_\delta\frac{1}{MN}\sum_{i=2}^{M}\sum_{j=2}^{N}\left[I(i,j)-I(i-1,j-1)\right]^2} \qquad (28)$$

and SDF is

$$SDF=\sqrt{w_\delta\frac{1}{MN}\sum_{j=1}^{N-1}\sum_{i=2}^{M}\left[I(i,j)-I(i-1,j+1)\right]^2} \qquad (29)$$

2.3.7 Phase Congruency

Phase congruency comprises of an absolute measure of image activity that defines the evaluation metric. The principal moments of the image phase congruency are used to define the metric because they contain the information for corners and edges. The metric is expressed as

$$Q_P=(P_p)^{\alpha}(P_M)^{\beta}(P_m)^{\gamma} \qquad (30)$$

where p, M, and m refer to phase congruency (p), maximum, and minimum moments, respectively;

$$P_p=max\left(C_{AF}^{p},C_{BF,}^{p}C_{SF}^{p}\right) \qquad (31)$$

$$P_M=max\left(C_{AF}^{M},C_{BF,}^{M}C_{SF}^{M}\right) \qquad (32)$$

$$P_m=max\left(C_{AF}^{m},C_{BF,}^{m}C_{SF}^{m}\right) \qquad (33)$$

where, $C_{xy}^{k},\{k\mid p,M,m\}$ is the correlation coefficient of the two sets x and y which is defined by:

$$C_{xy}^{k}=\frac{\sigma_{xy}^{k}+C}{\sigma_x^{k}\sigma_y^{k}+C'} \qquad (34)$$

$$\sigma_{xy}=\frac{1}{N-1}\sum_{i=1}^{N}(x_i-\bar{x})(y_i-\bar{y}) \qquad (35)$$

The suffixes A, B, F, and S correspond to the two inputs, the fused Image, and maximum-select map. The exponential parameters α, β, and γ can be adjusted based on the importance of the three components.

2.3.8 Piella's Metric

Piella's Metric uses the universal image quality index method to determine the local measure of an image *A*'s salience within window *w*, denoted *s*(*A*|*w*) to calculate a coefficient *c*(*w*) based on a ratio of max to sum considering both images involved. In this instance, *s*(*B*|*w*) is the salience within window w of image B and the local quality of A versus B is denoted Q(*A*,*B*|*w*). This term is then used to calculate the quality of the sliding window (Q_W) and put together finally to come up with the quality of the entire image:

$$Q_E = Q_W\left(A, B, F\right)\cdot Q_W\left(A', B', F'\right)^a \tag{36}$$

$Q_W(A',B',F')$ is the Q_w calculated with the edge images, *A', B',* and α is manually adjustable parameter to weight the edge-dependent information. Given the many transforms, image fusion methods, and image quality metrics, it is a challenge to determine which selection {Txm, ImgFus, IQmetric} is optimal for a given situation. The objective of this study is to compare and contrast these options in a comprehensive fashion.

III. RESULTS

To analyze the impact different transforms and fusions have on the quality representation value of the fused image, several subsets of the data were examined. A ranking system approach was used. The ranking approach stemmed from multiple comparison tests of factor effects models within each subset of data. This was done using the multi-comp library of R. The multi-comparison test is based on a design of experiments (DOE) approach to determine the independent and confounding factors.

There are some caveats in the analysis. It is important to note that the Bandelet data had no factor levels for the approximate coefficient variable, so if the factor effects model was fit with that variable, then the Bandelet data was omitted from the analysis. This was the only unfortunate drawback in what was otherwise a very effective way to compare factor levels within the data. Also, while the transform and detail coefficient analysis did not include the approximate coefficient factor parameter in the model; this provided a negligible effect on the difference of means comparisons because the means are averaged over all levels within the factors. The choice of the level averaging was considered to be better for the results of the study than omitting the Bandelet transformation data from the comparison tests. It should also be noted that, since the Bandelet does not have approximate coefficients, it would not have been a part of the comparison tests of approximate coefficients regardless.

When fitting factor effects to the models of the data, interaction terms were omitted due to covariate interaction. Thus the model is of the form:

$$Y_{ijk} = \mu.. + \alpha_i + \beta_j + \varepsilon_{ij} \tag{37}$$

where μ is the mean,αrepresentsthe transform, βrepresentsthe fusion method, and εis the residual error in the regression model.

Using the model, multiple comparisons GLHT were conducted using a Tukey adjustment to examine family-wise error rates. This means that for the transform study, with a 95% confidence, the probability of making at least one type 1 error (incorrect rejection of a true null hypothesis) will be 0.05 and that for any individual comparison the probability of a type 1 error is

$$\alpha = 1-(.95)^{\frac{1}{15}} \approx .003 \tag{38}$$

This is also the approximate probability of a type 1 error in any individual comparison in the fusion method study, as the exponent becomes 1/16. A type 1 error is the incorrect rejection of a true null hypothesis or a false positive.

3.1 Example LSMeans

Below, we show sample output for the GLHT for one transform comparison, under the phase congruency metric. The abbreviations used here are: Co for contourlet, Cu for Curvelet, DD for Double Density, DT for Dual Tree, W for Wavelet, and B for Bandelet. For each entry, the column index relates to the transform for the approximate coefficients and the row index relates to the transform for the detail coefficients.

```
        Simultaneous Tests for General Linear Hypotheses

Multiple Comparisons of Means: Tukey Contrasts


Fit: lm(formula = Value ~ Transform + Detail, data = pc)

Linear Hypotheses:
              Estimate Std. Error t value Pr(>|t|)
Co - B == 0   0.169847   0.013686  12.410   <0.001 ***
Cu - B == 0   0.283854   0.013686  20.740   <0.001 ***
DD - B == 0   0.233431   0.013686  17.056   <0.001 ***
DT - B == 0   0.212759   0.013686  15.546   <0.001 ***
W - B == 0    0.201965   0.013686  14.757   <0.001 ***
Cu - Co == 0  0.114007   0.006843  16.660   <0.001 ***
DD - Co == 0  0.063584   0.006843   9.292   <0.001 ***
DT - Co == 0  0.042912   0.006843   6.271   <0.001 ***
W - Co == 0   0.032117   0.006843   4.693   <0.001 ***
DD - Cu == 0 -0.050423   0.006843  -7.368   <0.001 ***
DT - Cu == 0 -0.071095   0.006843 -10.389   <0.001 ***
W - Cu == 0  -0.081890   0.006843 -11.967   <0.001 ***
DT - DD == 0 -0.020672   0.006843  -3.021   0.0278 *
W - DD == 0  -0.031466   0.006843  -4.598   <0.001 ***
W - DT == 0  -0.010795   0.006843  -1.577   0.5978
---
Signif. codes:  0 '***' 0.001 '**' 0.01 '*' 0.05 '.' 0.1 ' ' 1
(Adjusted p values reported -- single-step method)
```

Figure 9. Output for one iteration

Note that the *p*-values shown reflect a strong statistical probability (< 0.1%) that rejects the null hypothesis, meaning there was a significant difference in means of the values we compared. If we look at the first five rows of Figure 9, we can see that the Bandelet was outperformed by all five of the other transformations this method. Furthermore, if we consider the *p*-values, most of these numbers are very statistically significant. The only comparison that was not statistically

significant was Wavelet vs. Dual Tree With a t value (difference of means) of –1.577. In our approach to ranking the levels of each factor based on the results of the multiple comparisons test, a score was assigned to each level of each factor in two different manners. Consider the data above; a naïve scoring of the results would be to assign the numbers 1-6 to the rankings of the data in descending order as follows.

Table 1. Phase Congruency, naïve ranking points system

Rank	Transformation	Points
1	Curvelet	6
2	Double Density	5
3	Dual Tree	4
4	Wavelet	3
5	Contourlet	2
6	Bandelet	1

Though statistically naïve, this scoring system is still potentially useful. It indicates the ranking of the different algorithms, but it provides no information on the statistical significance of the rankings. One alternative system would be to adjust the points awarded based on statistical confidence; here we consider any result that does not achieve a 95% level of statistical confidence to be a tie and split the corresponding points accordingly. As noted above, the Dual Tree and Wavelet do not have a statistically significant difference. Therefore, we will share the points for the 3rd and 4th rankings evenly between the two resulting in the following scoring:

Table 2. Phase Congruency: significance adjusted ranking points

Rank	Transformation	Points
1	Curvelet	6
2	Double Density	5
3	Dual Tree	3.5
4	Wavelet	3.5
5	Contourlet	2
6	Bandelet	1

This can be done with any number of the rankings, not just two. For instance, Piella's metric yielded no significance for any of the comparisons in approximate coefficient fusion methods. Thus, for the adjusted scoring, each of those seven metrics received the score of 4 out of a possible 7.

3.2 Organization

When dealing with metric comparisons that have not been validated and are still not generally agreed upon, we examine the data in a number of ways in order to draw conclusions. We approached the data in order of certainty. First, approximate coefficients showed very little statistical significance, thus we consider them least when constructing inferences. When comparing transformations and detail coefficients, there is a more well-defined ranking of the transform data. Thus we use transform rankings to analyze the effectiveness of the metrics. Then we will look at the detail coefficient ranking in general, and what was effective across all transformations. Although useful, we may get even better results by only looking at the different detail coefficient when using the most effective transform. We will then repeat this with the different approximate coefficients comparing them while only using the most effective transforms and details

3.3 Transformation Comparison

The naïve and adjusted rankings for the transform comparisons are given in Tables 3 and 4. The Curvelet was the best performing transform in our study, as we can see from the following charts. A key point is that no matter the ranking system, the curvelet produced the top results for the metrics.

Just as the curvelet clearly distinguished itself atop the rankings, the contourlet was clearly the worst transform. We can see that the rankings don't change very significantly if we call ties for statistical insignificance, where only the Double density and the bandelet trade in various rankings. We can also see that based on this aggregate of all of the rankings in our study that the Wavelet came in second. This is interesting because all of the other transformations were developed with the intention of being improvements upon the Wavelet.

Table 3. Naïve Transform Rankings

Aggregate Rank	Transformation	Points
1	Curvelet	39
2	Wavelet	32
3	Bandelet	29
4	Double Density	27
5	Dual Tree	25
6	Contourlet	16

Table 4. Adjusted Transform Rankings

Aggregate Rank	Transformation	Points
1	Curvelet	35.5
2	Wavelet	34
3	Double Density	26.5
4	Bandelet	26
5	Dual Tree	25
6	Contourlet	21

When considering how closely the metrics rankings reflected the aggregate rankings, we see that Piella's metric was much different than the rest because it actually ranked the curvelet last, and it was the only transformation that ranked the contourlet in the top 3. We can also note that the only statistically significant difference it showed was the wavelet being better than the rest. This along with the fact that it found no significant contrast of means in the approximate coefficient data indicates that it has the most different results from the other metrics. Thus it would probably lend itself well to a receiver operating characteristic (ROC) validation study to see if it is not valid in this type of fusion. Alternatively, it could be the best metric for this type of fusion.

Additionally, we can consider the aggregate rankings and assign the scores 1-6 to those ranking just as we did for each set of rankings individually. Then by calculating the distance between this vector and each of the ranking vectors for the

metrics, we see that mutual information, Tsallis entropy, and the multiscale scheme were the closest rankings to our aggregate rankings. When we do the same considering the adjusted rankings, mutual information was the closest to being the same as the aggregates, while phase congruency was the second closest.

3.4 Detail Coefficient Comparison

Here we have a look at how the detail coefficients came up in the ranking analysis. We note that there is much less distinguishing the detail coefficients than there was the transformations. We can see that Down-Up was the best detail coefficient fusion method, but that all of the detail coefficient fusion methods were very close in score.

Table 5. Naïve Detail Coefficient Rankings

Aggregate Rank	Detail Fusion	Total Points
1	Down-Up	36
2	Mean	34
3	Up-Down	33
4	Min	32
5	Random	31
T6	Linear	29
T6	Max	29

Table 6. Adjusted Detail Coefficient Rankings

Aggregate Rank	Detail Fusion	Total Points
1	Down-Up	35
2	Min	33.5
3	Up-Down	32.5
4	Mean	32
5	Random	31
T6	Linear	30
T6	Max	29

It is interesting to note that phase congruency metric produced results that were all statistically significant. This means that perhaps it is the best at discerning differences between the detail coefficients. We also note that for the adjusted ranking system it had the smallest distance between its rankings vector and the aggregate rankings vector. Alternatively, Tsallis was by far the smallest distance in the naïve look at things, with phase congruency having the second smallest distance between the ranking vectors. It should also be noted that spatial frequency may indeed be best at identifying high quality detail fusion methods because it was the only method to rank the down-up method as the best and also determined that min was the second best. Here is a look at spatial frequency's rankings of the fusion methods:

Table 7. Spatial Frequency Detail Coefficient Rankings

Rank	Detail Fusion	Points
1	Down-Up	7
T2	Min	5.5
T2	Max	5.5
T4	Linear	3
T4	Random	3
T4	Up-Down	3
7	Mean	1

We can see that here max is tied for second with min, despite it turning up tied for last in our aggregate rankings. With the detail coefficient rankings all being so close, it seems that the transformation has more of an impact on quality measurements than the detail coefficient fusion does. Thus, the following study of detail coefficients with regards to just the curvelet transformation.

3.5 Approximate Coefficient Comparison

The following tables present the aggregate ranking results for the approximate coefficients. It is good to note that these showed the least statistical significance across the metrics of the different factors that were studied. This leads to the important insight that the approximate coefficients may be the least important factor in the quality of multi-focus fusion.

Table 8. Naïve Approximate Coefficient Rankings

Aggregate Rank	Approximate Coefficient	Total Points
1	Linear	42
2	Up-Down	41
3	Max	34
T4	Mean	33
T4	Down-Up	33
6	Min	27
7	Random	14

Table 9. Adjusted Approximate Coefficient Rankings

Aggregate Rank	Approximate Coefficient	Total Points
1	Linear	38.5
2	Min	34
3	Up-Down	33
4	Max	32
5	Mean	31
6	Down-Up	30
7	Random	25.5

The linear coefficient method of fusion distinguishes itself as the statistically significant strongest option for approximate coefficients. Meanwhile, we note that the rankings mix around a lot when comparing the naïve rankings and the adjusted rankings. With the only other agreement between the two sets of rankings being that the random method was the worst. This leads us to the observation that the linear approximate coefficient method is the safest choice when trying to optimize multi-focus fusion.

3.6 Insights from Curvelet

Since the curvelet was the best performing transformation, the fusion type that works best with itis of particular interest. In the following table, we can see the results for the detail coefficient rankings for the curvelet:

Table 10. Naïve Detail Coefficient Rankings, Curvelet

Aggregate Rank	Detail Coefficient	Total Points
1	Linear	37
2	Down-Up	35
T3	Mean	34
T3	Random	34
T3	Min	34
6	Up-Down	28
7	Max	22

Table 11. Adjusted Detail Coefficient Rankings, Curvelet

Aggregate Rank	Detail Coefficient	Total Points
1	Down-Up	36.5
T2	Linear	33.5
T2	Mean	33.5
4	Random	31
T5	Max	30
T5	Up-Down	30
7	Min	29.5

Here we can see that down up, linear, and mean were the three most effective detail coefficients when working solely with the curvelet. When we consider the statistical significance of the rankings we can see that Down-Up is the most effective. It would perhaps be useful to compare them with rankings from a human subjective evaluation to differentiate which is the best to pair with the curvelet.

The approximate coefficients appeared to be much less statistically significant with only three adjacent ranking differences being statistically significant total over the rankings using all eight of the metrics. Nonetheless, here is our aggregate result for approximate coefficients:

Table 12. Naïve Approximate Coefficient Rankings, Curvelet

Aggregate Rank	Approximate Coefficient	Total Points
1	Linear	44
2	Down-Up	37
T3	Mean	34
T3	Random	34
5	Min	29
6	Up-Down	26
7	Max	20

Table 13. Adjusted Approximate Coefficient Rankings, Curvelet

Aggregate Rank	Approximate Coefficient	Total Points
1	Linear	35
T2	Down-Up	31.5
T2	Mean	31.5
T2	Random	31.5
T2	Min	31.5
T2	Up-Down	31.5
T2	Max	31.5

Although there was not a lot of clear differentiation between the approximate coefficients, it is a safe choice to select linear approximate coefficients when fusing images with the curvelet.

IV. CONCLUSIONS

The study sought to investigate six contemporary transforms, seven fusion methods, and eight image quality metrics for multi-focus image fusion. Insights from the study revealed that the curvelet was the only one of the transformations designed to improve upon the wavelet that demonstrated an improvement for multi-focus image fusion. When analyzing the detail coefficients, the data indicates that down-up is the best suited for multi-focus fusion, being the optimal choice when considering all transformations as well as the best in the statistically significant study when only considering the curvelet numbers. It is clear that linear was the best performing approximate coefficient in our study, among all of the transformations and when the data was just restricted to just the curvelet transformation. When considering metrics, Tsallis distinguished itself as most closely following the aggregate rankings that were produced. This leads us to believe that it may be the best indicator of visual quality of a multi-focus fusion. Additional comparison with human subjective ratings should be used in the future to confirm that this is the case.

Future work for image fusion comparison should be centered on the unification of image fusion metrics into a single automated fusion system that can use the results of this study and others to determine and carry out the optimal fusion by choosing the correct transformation method, approximate coefficient method, and detail coefficient method. Additional studies should be conducted to include the use of additional fusion types, including those that work with different modalities and sensor types.

Acknowledgements

The authors would like to extend their gratitude to Indiana University of Pennsylvania's students David Kornish, Michael McLaughlin, Justin Fleming, Colter Long, Sam Greggs and Joseph Stango for the integration of the MATLAB code and work on the project. The authors also extend their gratitude to Dr. Erik Blasch at the Air Force Research Lab for his technical contribution.

References

[1] Peng, Kewu, and John C. Kieffer. "Embedded image compression based on wavelet pixel classification and sorting." *IEEE Transactions on Image Processing* 13, no. 8 (2004): 1011-1017.

[2] Chrysafis, Christos, and Antonio Ortega. "Line-based, reduced memory, wavelet image compression." *IEEE Transactions on Image processing* 9, no. 3 (2000): 378-389.

[3] Efstratiadis, Serafim N., Dimitrios Tzovaras, and Michael G. Strintzis. "Hierarchical partition priority wavelet image compression." *IEEE transactions on image processing* 5, no. 7 (1996): 1111-1123.

[4] Lin, En-Ui, Michael McLaughlin, and Abdullah Ali Alshehri. "Medical image segmentation using multi-scale and super-resolution method." In *2014 IEEE Applied Imagery Pattern Recognition Workshop (AIPR)*, pp. 1-5. IEEE, 2014.

[5] Daubechies, Ingrid. *Ten lectures on wavelets*. Vol. 61. Philadelphia: *Society for industrial and applied mathematics*, 1992.

[6]Selesnick, Ivan W., Richard G. Baraniuk, and Nick C. Kingsbury. "The dual-tree complex wavelet transform." *IEEE signal processing magazine* 22, no. 6 (2005): 123-151.

[7] Gnanadurai, D., and V. Sadasivam. "Image de-noising using double density wavelet transform based adaptive thresholding technique." *International Journal of Wavelets, Multiresolution and Information Processing* 3, no. 01 (2005): 141-152.

[8] Saevarsson, Birgir Bjorn, Johannes R. Sveinsson, and Jon Atli Benediktsson. "Time invariant curvelet denoising." In *Proceeding of the Nordic Signal Processing Symposium,(NORSIG 2004)*, vol. 117120. 2004.

[9] Do, Minh N., and Martin Vetterli. "The contourlet transform: an efficient directional multiresolution image representation." *IEEE Transactions on image processing* 14, no. 12 (2005): 2091-2106.

[10] Mallat, Stéphane, and Gabriel Peyré. "Orthogonal bandlet basesforgeometric images approximation." *Communications on Pure and Applied Mathematics* 61, no. 9 (2008): 1173-1212.

[11] Le Pennec, Erwan, and Stephane Mallat. "Bandelet image approximation and compression." *Multiscale Modeling & Simulation* 4, no. 3 (2005): 992-1039.

[12] Qu, Xiaobo, Jingwen Yan, Guofu Xie, Ziqian Zhu, and Bengang Chen. "A novel image fusion algorithm based on bandelet transform." *Chinese Optics Letters* 5, no. 10 (2007): 569-572.

[13] Moore, Ryan, Soundararajan Ezekiel, and Erik Blasch. "Denoising one-dimensional signals with curvelets and contourlets." In *NAECON 2014-IEEE National Aerospace and Electronics Conference*, pp. 189-194. IEEE, 2014.

[14] McLaughlin, Michael J., En-Ui Lin, Erik Blasch, Adnan Búbalo, Maria Cornacchia, Mark Alford, and Millicent Thomas. "Multi-resolution deblurring." In *2014 IEEE Applied Imagery Pattern Recognition Workshop (AIPR)*, pp. 1-6. IEEE, 2014.

[15] Yang, Ronggen, and Mingwu Ren. "Wavelet denoising using principal component analysis." *Expert Systems with Applications* 38, no. 1 (2011): 1073-1076.

[16] Gnanadurai, D., V. Sadasivam, J. Paul Tiburtius Nishandh, L. Muthukumaran, and C. Annamalai. "Undecimated double density wavelet transform based speckle reduction in SAR images." *Computers & Electrical Engineering* 35, no. 1 (2009): 209-217.

[17] Papageorgiou, Constantine, and Tomaso Poggio. "A trainable system for object detection." *International Journal of Computer Vision* 38, no. 1 (2000): 15-33.

[18] Kingsbury, Nick. "The dual-tree complex wavelet transform: a new efficient tool for image restoration and enhancement." In *Signal Processing Conference (EUSIPCO 1998), 9th European*, pp. 1-4. IEEE, 1998.

[19] Liu, Chao-Chun, and Dao-Qing Dai. "Face recognition using dual-tree complex wavelet features." *IEEE Transactions on Image Processing* 18, no. 11 (2009): 2593-2599.

[20] Wang, Xiang-Yang, and Zhong-Kai Fu. "A wavelet-based image denoising using least squares support vector machine." *Engineering Applications of Artificial Intelligence* 23, no. 6 (2010): 862-871.

[21] Ezekiel, Soundararajan, Kyle Harrity, Erik Blasch, and Adnan Bubalo. "No-reference blur metric using double-density and dual-tree two-dimensional wavelet transformation." In *NAECON 2014-IEEE National Aerospace and Electronics Conference*, pp. 109-114. IEEE, 2014.

[22] McLaughlin, Michael J., Samuel Grieggs, Soundararajan Ezekiel, Michael H. Ferris, Erik Blasch, Mark Alford, Maria Cornacchia, and Adnan Bubalo. "Bandelet denoising in image processing." In *2015 National Aerospace and Electronics Conference (NAECON)*, pp. 35-40. IEEE, 2015.

[23] Giansiracusa, Michael, Adam Lutz, Soundararajan Ezekiel, Mark Alford, Erik Blasch, Adnan Bubalo, and Millicent Thomas. "Multi-focus and multi-modal fusion: a study of multi-resolution transforms." In *SPIE Defense+ Security*, pp. 98410I-98410I. International Society for Optics and Photonics, 2016.

[24] Ferris, Michael H., Michael McLaughlin, Samuel Grieggs, Soundararajan Ezekiel, Erik Blasch, Mark Alford, Maria Cornacchia, and Adnan Bubalo. "Using ROC curves and AUC to evaluate performance of no-reference image fusion metrics." In *2015 National Aerospace and Electronics Conference (NAECON)*, pp. 27-34. IEEE, 2015.

[25] Liu, Zheng, Erik Blasch, Zhiyun Xue, Jiying Zhao, Robert Laganiere, and Wei Wu. "Objective assessment of multiresolution image fusion algorithms for context enhancement in night vision: a comparative study." *IEEE transactions on pattern analysis and machine intelligence* 34, no. 1 (2012): 94-109.

[26] Candes,Emmanuel Jean. "Ridgelets: theory and applications." PhD diss., Stanford University, 1998.

[27] Starck, Jean-Luc, Emmanuel J. Candès, and David L. Donoho. "The curvelet transform for image denoising." *IEEE Transactions on image processing* 11, no. 6 (2002): 670-684.

[28] Tsai, Wei-shi. "Project White Paper-Contourlet Transforms for Feature Detection." (2008).

[29] Sveinsson, Johannes R., and Jon Atli Benediktsson. "Combined wavelet and contourlet denoising of SAR images." In *IGARSS 2008-2008 IEEE International*

Geoscience and Remote Sensing Symposium, vol. 3, pp. III-1150. IEEE, 2008.

[30] Xingmei, Li, Yan Guoping, and Chen Liang. "A new method of image denoise using contourlet transform." In *Environmental Science and Information Application Technology, 2009. ESIAT 2009. International Conference on*, vol. 2, pp. 390-393. IEEE, 2009.

[31] Harrity, Kyle, Soundararajan Ezekiel, Michael Ferris, Maria Cornacchia, and Erik Blasch. "No-reference multi-scale blur metric." In *NAECON 2014-IEEE National Aerospace and Electronics Conference*, pp. 103-108. IEEE, 2014.

[32] Tzeng, Jack, Chun-Chen Liu, and Truong Q. Nguyen. "Contourlet domain multiband deblurring based on color correlation for fluid lens cameras." *IEEE Transactions on Image Processing* 19, no. 10 (2010): 2659-2668.

[33] Choi, Yoonsuk, Ershad Sharifahmadian, and Shahram Latifi. "Performance analysis of contourlet-based hyperspectral image fusion methods."*International Journal on Information Theory* 2, no. 1 (2013): 1-14.

[34] Liu, Zheng, and Erik Blasch. "Statistical analysis of the performance assessment results for pixel-level image fusion." In *Information Fusion (FUSION), 2014 17th International Conference on*, pp. 1-8. IEEE, 2014.

[35] Messer, Neal, Soundararajan Ezekiel, Michael H. Ferris, Erik Blasch, Mark Alfor, Adnan Bubalo, and Maria Cornacchia. "ROC Curve Analysis for Validating Objective Image Fusion Metrics." *2015 Applied Image Patter Recognition Workshop (AIPR)*, IEEE, 2015.

[36] Giansiracusa, Michael, Adam Lutz, Soundararajan Ezekiel, Mark Alford, Erik Blasch, Adnan Bubalo, and Millicent Thomas. "Bandelet-based image fusion: a comparative study for multi-focus images." *2016 Geospatial Informatics, Fusion, and Video Analytics VI, SPIE Defense + Security Conference*, IEEE, 2016

[37] Lutz, Adam, Kendrick Grace, Neal Messer, Soundararajan Ezekiel, Erik Blasch, Mark Alford, Adnan Bubalo, and Maria Cornacchia. "Bandelet Transformation based Image Registration."*2015 Applied Image Patter Recognition Workshop (AIPR)*, IEEE, 2015.

[38] Lutz, Adam, Michael Giansiracusa, Neal Messer, Soundararajan Ezekiel, Erik Blasch, and Mark Alford. "Optimal multi-focus contourlet-based image fusion algorithm selection."*2016 Geospatial Informatics, Fusion, and Video Analytics VI, SPIE Defense + Security Conference*, IEEE, 2016